

Note: this paper is a non-peer reviewed preprint submitted to EarthArXiv. The authors welcome feedback as it undergoes substantial revisions before submission to a peer-reviewed journal.

Assessing Climate Model Projections of Anthropogenic Warming Patterns

Henri F. Drake (henrifdrake@gmail.com)^{*1,2}

Tristan Abbott (thabbott@mit.edu)¹

Megan Lickley (mlickley@mit.edu)¹

¹Massachusetts Institute of Technology, Cambridge, MA, USA

²Woods Hole Oceanographic Institution, Woods Hole, MA, USA

1 **Projections of future anthropogenic climate change and their uncertainties are determined by analyzing large**
2 **ensembles of numerical climate models [1]. Since the late 1980s, transient climate models have projected a**
3 **pronounced global warming, with relatively high warming in the Arctic and over land and low warming over**
4 **the Southern Ocean [e.g. 2]. In general, confidence in climate model projections is based on their representa-**
5 **tions of physical processes and on how well they reproduce past climates [3]. However, the relationship between**
6 **a model’s ability to reproduce past climate changes and project future climate changes is unknown, as ob-**
7 **servations of the future are by definition unavailable. Here, we assess climate model projections of ‘future’**
8 **global warming patterns published in the 1995 Intergovernmental Panel on Climate Change Second Assess-**
9 **ment Report by quantitatively comparing them to observations acquired between 1990 and 2018 [4, 5]. Ob-**
10 **servated patterns of warming follow model projections, falling within 1.64 inter-model standard deviations of the**
11 **multi-model mean over most of the globe, with the exception of the West Pacific and Southern Oceans where we**
12 **observe regional cooling trends associated with the ‘global warming hiatus’ [6]. We find a correlation between a**
13 **model’s ability to reproduce spatially-resolved temperature trends over the 1920-1990 hindcast period and the**
14 **1990-2018 ‘nowcast’ period, increasing our confidence in their projections of the future and lending support to**
15 **Bayesian approaches in climate modelling [7]. Climate change mitigation has now been delayed long enough**
16 **for the first projections of anthropogenic global warming to be borne out in observations, dismissing claims that**
17 **models are too inaccurate to be useful and reinforcing calls for climate action [8].**

18 There are a variety of approaches for assessing general circulation models (GCMs) based on the fidelity with which
19 they simulate past climate (hindcast skill), but little understanding as to how these assessments relate to the fidelity of
20 their projections of future climate (forecast skill) [See Methods for a brief review of approaches and their respective
21 limitations]. Because of this gap in understanding, it is worth revisiting projections from early generations of climate
22 models for which we now have contemporary observations to probe the relationship between model hindcast skill and
23 model forecast skill. These models provide the data required for an ideal GCM verification experiment: an observed
24 forecast period (henceforth referred to as a ‘nowcast’ to distinguish it from the unobserved 1990-2100 ‘forecast’
25 period) spanning a time frame long enough for long-term trends to emerge above the noise of inter-annual variability
26 [9]. In the tropics and Arctic, the projected time of emergence is roughly 30-50 years for surface air temperature trends
27 for a signal to noise ratio of 2 [10], suggesting that nowcast verification experiments may already be possible for model
28 projections that begin around 1990. The earliest GCM projections of anthropogenic climate change due to both the
29 warming tendency of greenhouse gas (GHG) emissions and the cooling tendency of sulfate aerosol emissions begin in
30 1990 and are described by the 1995 Intergovernmental Panel on Climate Change (IPCC) in their Second Assessment
31 Report (SAR) [4]. (See Methods for a description of the SAR models.) Here, we revisit the SAR’s decades-old
32 climate model simulations to assess the accuracy of their ‘future’ projections and to develop a framework for using
33 skill metrics to quantify the relationship between climate model hindcast skill and forecast skill.

34 The projected increase of radiative forcing in the SAR is of similar magnitude to modern best estimates of historical
35 forcings, allowing us to compare the SAR models’ response with the observed climate response (Figure 1, right).

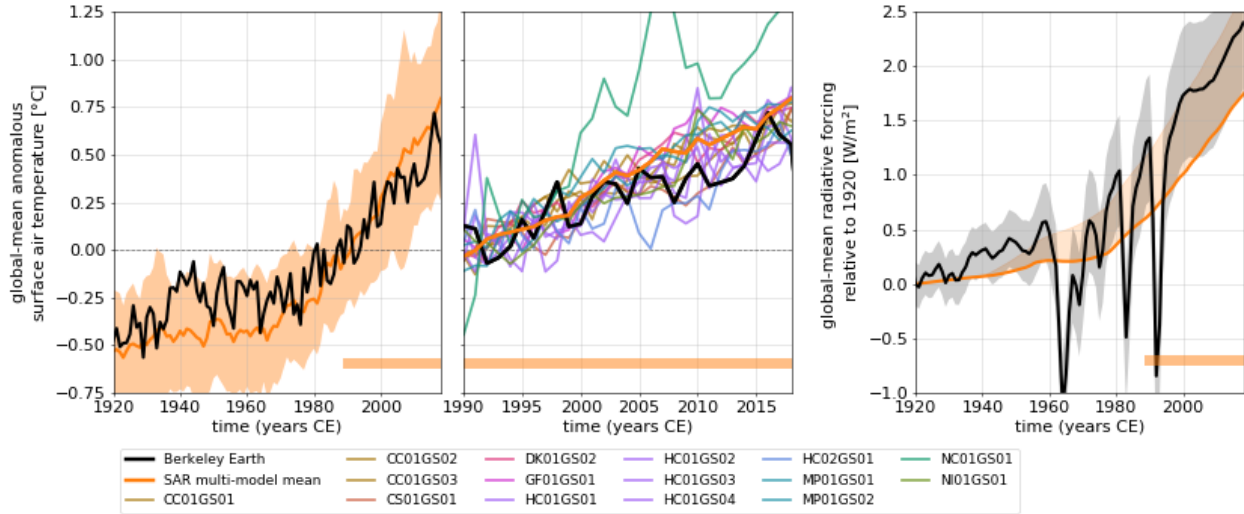


Figure 1: Projected and observed global annual mean surface air temperature anomalies and radiative forcing. (Left) Global annual mean surface air temperature anomalies relative to the 1985-1995 mean. Solid lines show the (black) Berkeley Earth observations and (orange) SAR multi-model mean. Orange shading shows the SAR multi-model mean $\pm\zeta$, where ζ is the inter-model standard deviation. (Middle) Global annual mean surface air temperature anomalies relative to the 1985-1995 mean for each individual SAR model, where colors indicate different models. (Right) Global mean radiative forcing relative to 1920. Solid lines show our estimates of historical and SAR model forcing and shading shows uncertainty estimates (see Methods for details). The orange bars delineate the 1990-2018 nowcast period.

36 The SAR multi-model mean accurately reproduces the observed global-mean warming over a 1920-1990 hindcast
 37 period and accurately projects the observed global-mean warming over the 1990-2018 nowcast period (Figure 1, left).
 38 All individual models exhibit global-mean warming and inter-annual variability similar to the observations over the
 39 1990-2018 nowcast period, except the NC01GS01 outlier model (Figure 1, middle). However, the agreement between
 40 the modelled and observed global-mean warming may be the spurious result of compensation between positive and
 41 negative biases (e.g. high climate sensitivity and low aerosol forcing [11] or high GHG forcing and high aerosol forcing
 42 [12]). Since different forcing agents have different patterns of forcing (e.g. aerosol forcing is more localized than
 43 GHG forcing), one might expect that analyzing spatial patterns of temperature trends allows for a more meaningful
 44 assessment of model skill [13]. The dependence of the temperature response pattern on the forcing patterns is muddled,
 45 however, by a relatively stronger dependence of the temperature pattern on local feedback patterns [14].

46 Observations during the 1990-2018 nowcast period show spatially varying temperature trends and regional emergence
 47 of warming over much but not all of the globe (Figure 2 A). We observe Arctic amplification with Arctic temperature
 48 trends of approximately 2°C and warming that emerges throughout much of the Arctic despite large inter-annual tem-
 49 perature variability (Figure 2 C). Temperature increases of approximately 1°C are common throughout both the tropics

50 and midlatitudes, but the emergence of warming is confined largely to the tropics where inter-annual variability is small
 51 [10]. The primary exceptions to the midlatitude and tropical warming trends are: cooling in the Equatorial Pacific,
 52 the North Pacific, and Northern Eurasia (associated with natural modes of variability [6] during the ‘hiatus’ period or
 53 changes in patterns of aerosol loading [15]); cooling in the North Atlantic (possibly associated with forced changes
 54 in the Atlantic Meridional overturning circulation [16]); and cooling in the Southern Ocean (possibly associated with
 55 forced changes in ocean circulation [17] or underestimated natural variability [18]).

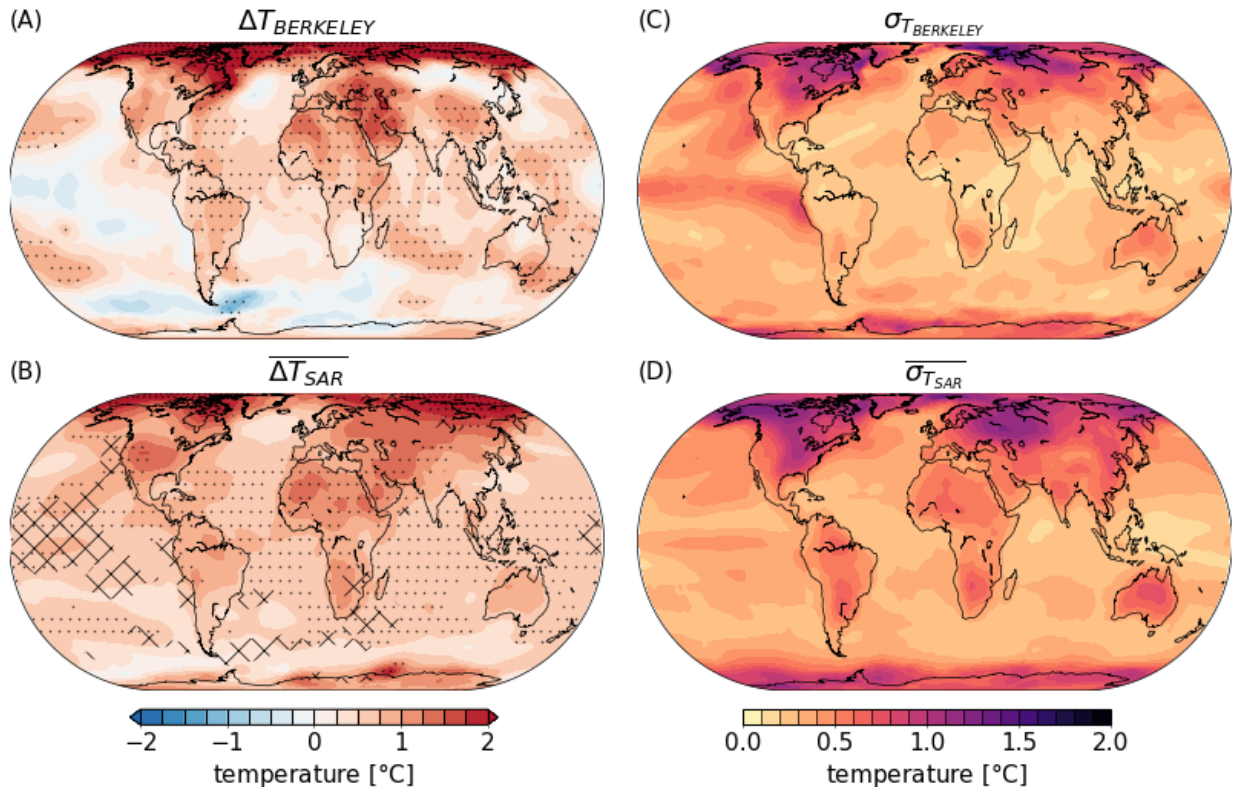


Figure 2: Observed and projected spatial patterns of temperature linear trends (expressed as a temperature change over the 28 year nowcast period) and inter-annual temperature variability over the 1990-2018 nowcast period, linearly interpolated onto a common 3° by 3° grid. (Left) Spatial patterns of temperature trends and (Right) inter-annual variability σ , defined as the standard deviation of the annual-mean temperature timeseries with the nowcast linear trend removed, for: (A, C) the Berkeley Earth observational data set and (B, D) the SAR multi-model mean. Stippling shows where the absolute temperature trend signal has emerged above the noise of inter-annual variability, $|\Delta T| > 2\sigma$, following [10, 19]. For visual clarity, we only show stippling at every other grid cell longitude and every other grid cell latitude. Hatching shows where the observations fall outside of $\overline{\Delta T_{\text{SAR}}} \pm 1.64\zeta$, where ζ is defined as the inter-model standard deviation in linear temperature trends and $\overline{\Delta T_{\text{SAR}}}$ is the multi-model mean temperature trend.

56 The projected SAR multi-model mean (MMM) temperature trends agree with the Berkeley Earth observations within
 57 inter-model uncertainty ΔT_{SAR} over the nowcast period over most of the globe, except in the West Pacific and the Southern

58 Ocean (Figure 2 B). The MMM warming trend emerges over noise throughout the tropics largely as a result of weak
59 inter-annual variability, as in the observations. The MMM Arctic warming trend is weaker than the observed trend and
60 emerges above noise over less of the high-latitude northern hemisphere, but still agrees with observations to within
61 uncertainty. The MMM projects anomalously weak warming rather than cooling in the Southern Ocean and does not
62 project the hiatus-period West Pacific cooling signal seen in observations. Inter-model averaging is largely responsible
63 for muted spatial variability: some but not all individual models produce widespread patterns of warming and limited
64 regional cooling qualitatively similar to those seen in observations (Extended Data Figure 1) [as in 20]. The MMM
65 exhibits a clear land-ocean warming contrast, as do some but not all individual models [21].

66 Some individual models project temperature trends over the nowcast period more accurately than others (Extended
67 Data Figure 1); can their nowcast skill be predicted based on their hindcast skill? To quantify the relationship between
68 hindcast skill and nowcast skill, we compute skill metrics based on the global mean root-mean-squared model error
69 with respect to Berkeley Earth observations for each model over the hindcast and nowcast periods [as in refs. 1, 22] (See
70 Methods for skill metric definitions). We choose this skill metric as it reflects how well model projections capture both
71 the magnitude and spatio-temporal patterns of observed temperature changes. We compute hindcast skill metrics based
72 on three spatially resolved temperature-related fields: linear trends (TREND), annual-mean anomalies of the detrended
73 signal (ANOM), and a climatology of seasonal cycles relative to their respective annual means (SEASON). We choose
74 these metrics to identify skill in simulating processes on decadal, annual, and monthly timescales, respectively. To
75 highlight the information added by considering spatial patterns of trends rather than global-mean temperature trends,
76 we also compute a hindcast skill metric based on the absolute error in global-mean temperature trends (GLOBAL). We
77 compare all four hindcast skill metrics to the TREND metric applied to the nowcast (Figure 3). The hindcast ANOM
78 metric, pertaining to inter-annual variability, is the metric best correlated with the nowcast TREND metric (Figure 3,
79 C), suggesting the importance of internal modes of variability such as the Pacific Decadal Oscillation and El-Niño
80 Southern Oscillation over the hindcast period to spatial patterns of temperature trends over the nowcast period [6].
81 The TREND metrics for the hindcast and nowcast periods are also correlated (Figure 3, A) and are robust to changes
82 in the length of the hindcast interval (Figure 5, left), supporting the intuitive assumption that models which reproduce
83 historical temperature trends are more likely to accurately project future temperature trends. The GLOBAL and
84 SEASON metrics for the hindcast are poorly correlated with the TREND metric for the nowcast (Figure 3, B and D).
85 The strong correlation between hindcast skill and forecast skill for the outlier model suggests that errors in multi-model
86 mean projections could be reduced by ignoring outlier models that perform poorly on hindcast. Even with the outlier
87 model included, though, the MMM outperforms any individual model over both the hindcast and forecast periods for
88 all but the GLOBAL metric, supporting the common practice of using the MMM as a ‘best guess’ projection [1]. On
89 the relatively short timescale of the nowcast period, however, the MMM’s exceptional skill may be attributable to the
90 attenuation of internal variability by ensemble-averaging, while individual models are instead penalized for exhibiting
91 modes of variability out of phase with observed variability [20]. The positive correlations we find between model skill
92 over the hindcast and nowcast periods support the community’s push towards Bayesian methods of analysing climate
93 model ensembles [7].

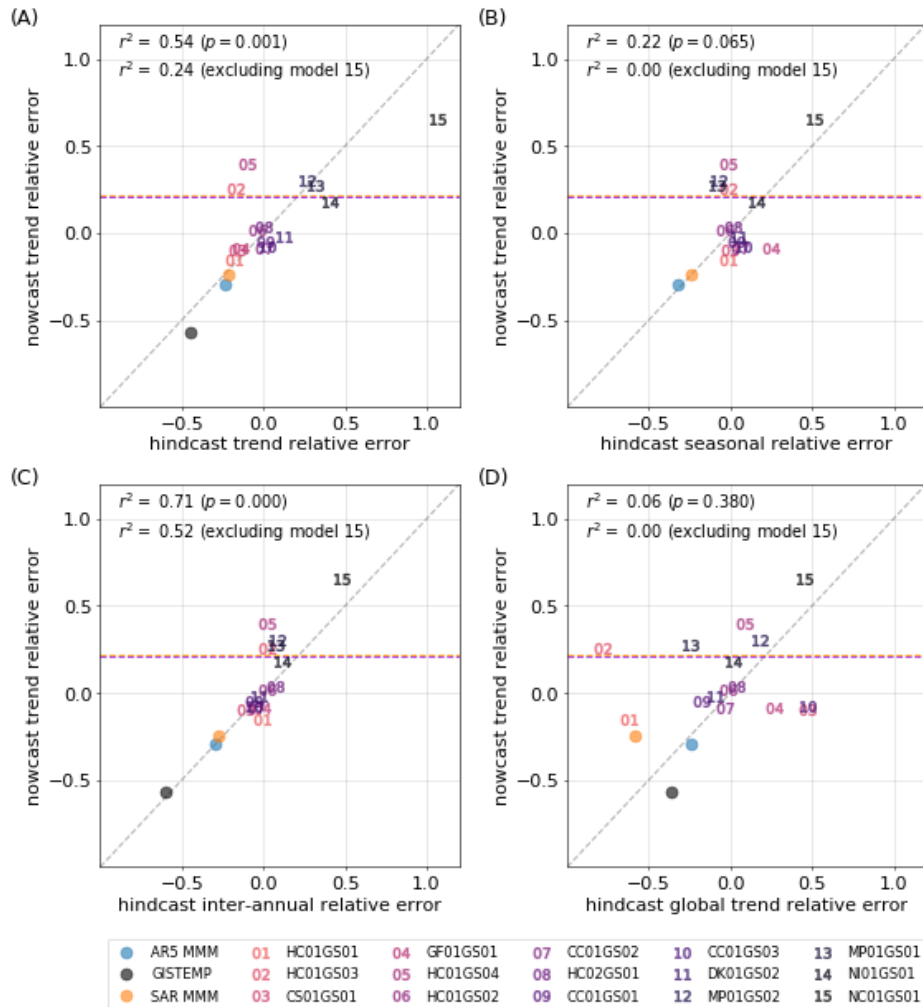


Figure 3: Correlations between skill metrics for the 1920-1990 hindcast and 1990-2018 nowcast. Y-axes show the skill metric pertaining to spatially-resolved temperature trends for the nowcast. The x-axes show four skill metrics for the hindcast: (A) a spatially-resolved temperature trend metric TREND, (B) a temperature seasonality metric SEASON, (C) an inter-annual temperature variability metric ANOM, and (D) a global-mean temperature trend metric GLOBAL (see Methods for details). Large negative values indicate high model skill, with a value of -1 indicating exact agreement with the Berkeley Earth observations. We show (blue) the AR5 multi-model mean, (black) the GISTEMP observations, (orange) the SAR multi-model mean, and (1-15) each individual SAR model. Coefficients of determination r^2 are calculated (upper) by excluding GISTEMP and the AR5 multi-model mean and (lower) additionally excluding the outlier model NC01G501. The nearly overlapping colored dashed lines show values of the nowcast spatially-resolved temperature trend metric for two reference cases: (purple) zero trend in every grid cell and (orange) linearly extrapolating the Berkeley Earth hindcast trend patterns to the nowcast period. Note that the AR5 1990-2018 ‘nowcast’ metric represents a combination of hindcast and nowcast since its forcing projections begin in 2005.

94 To benchmark the absolute skill of SAR models, we compare them to two heuristic projections of warming patterns
95 for the nowcast: 1) uniformly-zero temperature trends and 2) a linear extrapolation of observed hindcast temperature
96 trends at each grid cell (see Extended Data Figure 2, A). The MMM and most individual model projections are more
97 skillful than both heuristic models (Figure 3, colored lines), independent of the length of the hindcast period used
98 for extrapolation (Extended Data Figure 5, right). We also include a second observational product (the GISTEMP
99 temperature dataset) as a reference point to illustrate the degree of uncertainty in our observational dataset and to
100 indicate the potential for model improvement. Hindcast skill is slightly improved in the IPCC Fifth Assessment Report
101 (AR5) MMM relative to the SAR MMM (Figure 3), suggesting incremental improvements in modelling hindcast
102 temperature trends [23][see Methods for a description of the AR5 models]. We note that the incremental improvements
103 between the SAR and AR5 may be due to an upper limit on hindcast skill set by the stochastic phasing of internal
104 variability.

105 Our results build confidence in the ability of numerical climate models to project patterns of anthropogenic global
106 warming on multi-decadal timescales. With every climate model generation come improvements in both the reso-
107 lution and parameterization of climate-relevant processes [1]. Whether increasingly comprehensive climate models
108 produce more accurate projections, however, is yet to be determined [3]. To facilitate this future work, we encourage
109 modelling centers to archive model source code and documentation so that simulations can be re-run in their original
110 configurations (i.e. parameter values and initial conditions) but with realized forcing scenarios prescribed retrospec-
111 tively. Such retrospective simulations would allow errors in the projected climate response to be deconvoluted from
112 errors in the projected radiative forcing, providing a more robust framework for the verification and inter-generational
113 comparison of climate model projections. The respective contributions of internal variability and the forced response to
114 the skill of multi-decadal model predictions could be disentangled by using ‘dynamical adjustment’ techniques which
115 remove temperature anomalies induced by circulation anomalies and therefore approximate the observed and modelled
116 forced response [24]. We expect further insights into climate model forecast skill to be gained as the first generation of
117 coordinated decadal predictions, simulations which are initialized with observed phases of internal variability, reach
118 maturity [25].

119 **Methods**

120 **Approaches to climate model assessment**

121 A straightforward approach to assessing climate models is to compare spatial patterns of simulated and observed fields
122 over the hindcast period [eg. 26, 27]. For large model ensembles or a large number of climate variables, a common
123 approach involves computing scalar metrics that assess model hindcast skill and can be compared across models in an
124 ensemble, across different climate variables, and across model generations [3, 22, 28]. The implicit assumption in both
125 approaches is that a GCM’s skill at reproducing the observed past climate provides an indication of its overall physical

126 representation of the climate system and thus its ability to forecast future climate. This, however, raises the question
127 of whether tuning GCM parameters to reproduce the hindcast period introduces compensating model errors [29–31].
128 In the limit of excessive tuning, high hindcast skill may become uncorrelated (or even negatively correlated) with
129 forecast skill. Since successive model generations perform better at such skill metrics, it is argued that “an increasing
130 level of confidence can be placed in model-based predictions of climate”, with the caveat that this is “only true to the
131 extent that the performance of a model in simulating present mean climate is related to the ability to make reliable
132 forecasts of long-term trends” [3]. One of our novel contributions is to quantify this relationship for temperature trends
133 on multi-decadal timescales.

134 Models have also been evaluated based on their ability to reproduce paleoclimates given estimated boundary conditions
135 [32, 33]. Estimates of paleoclimate are considered ‘out-of-sample’ verification data because models are generally
136 developed and tuned in the context of the historical hindcast period. However, this approach is limited by both
137 uncertainties in past climate states and the viability of past climate states as analogues of transient anthropogenic
138 climate change [33, 34].

139 Some models have demonstrated skill in forecasting the short term climate response to a pulse of radiative forcing,
140 such as the volcanic eruption of Pinatubo in 1991 [eg. 35, 36]. However, it is unclear how skill in such exercises
141 relate to skill at forecasting a multi-decadal response to sustained anthropogenic forcing. The earliest multi-decadal to
142 centennial GCM forecasts are now being verified with respect to ensuing observations, but comparisons documented
143 in the literature to date are either qualitative [37] or limited to global-mean variables [38, 39].

144 **IPCC Second Assessment Report (SAR) Models**

145 The following are the subset of coupled atmosphere-ocean general circulation models in the IPCC Second Assessment
146 Report (SAR)[4] which have output archived in the IPCC data distribution center ([http://www.ipcc-data.org/
147 sim/gcm_monthly/IS92A_SAR/index.html](http://www.ipcc-data.org/sim/gcm_monthly/IS92A_SAR/index.html)): ECHAM3/OPYC3 (DK01) from the German Climate Computing
148 Center [40–42]; ECHAM4/OPYC3 (MP01) from Germany’s Max Plank Institute for Meteorology [40–42]; HADCM2
149 (HC01) and HADCM3 (HC02) from the UK’s Hadley Center for Climate Prediction and Research [43, 44]; CSIRO-
150 Mk2 (CS01) from Australia’s Commonwealth Scientific and Industrial Research Organization [45]; NCAR-CESM
151 (NC01) from the USA’s National Center for Atmospheric Research [46]; GFDL-R15 (GF01) from the USA’s Geo-
152 physical Fluid Dynamics Laboratory [21, 47]; CGCM1 (CC01) from Canada’s Center for Climate Modelling and
153 Analysis [48, 49]; CCSR/NIES AOGCM (NI01) from Japan’s Center for Climate System Research and National In-
154 stitute for Environmental Studies [50, 51]. All of the SAR models contain coupled and dynamic ocean, atmosphere,
155 and sea-ice models. All models are flux-adjusted to avoid drift in the model mean state, except for NC01 which does
156 not use any flux adjustments. All models are linearly interpolated to a 3° latitude by 3° longitude grid. These model
157 runs predate the Coupled Model Intercomparison Project (CMIP), although many models are similar to versions used
158 in CMIP1 (preindustrial control runs with constant radiative forcings) and CMIP2 (forced by 1%/year compound in-

159 crease in CO₂ concentrations).

160

161 We consider SAR simulations which are forced by changes in both greenhouse gas (GHG) and sulfate aerosol con-
162 centrations. Aerosol forcings are parameterized as an increased surface albedo and represent only the aerosol direct
163 effect. Most models approximate the radiative forcing of all GHGs with an equivalent CO₂ concentration, though
164 some perform radiative transfer calculations for each individual gas. Before 1990, the SAR models are forced by
165 historical GHG and anthropogenic sulfate aerosol concentrations. After 1990, GHG and aerosol concentrations evolve
166 according to the IS92a scenario [52]. The IS92a represents a scenario in which population rises to 11.3 billion by
167 2100, economic growth averages 2.3% per year, and energy is produced by a mix of fossil fuel and renewable sources,
168 resulting in a total anthropogenic forcing of about 6 W/m² above preindustrial levels by 2100. Changes in forcing due
169 to volcanic eruptions, solar variability, and orbital oscillations are excluded in both the 1920-1990 hindcast and the
170 1990-2100 forecast periods. We choose to start our nowcast period in 1990 (when forcings switch from historical to
171 projected) rather than 1996 (the SAR publication year), but our results are qualitatively similar if we instead choose to
172 consider a 1996-2018 nowcast period. Since radiative forcing data was not archived for the SAR models, we estimate
173 their forcing by digitizing offline calculations IS92a scenario radiative forcing from figure 6.18 of the SAR (Figure 1,
174 solid orange line in right panel). Since these offline calculations include the indirect effect of aerosols on clouds that is
175 not included in the SAR models, we estimate a correction to the SAR forcing by subtracting the timeseries of indirect
176 effect forcing in Figure 6.19 of the SAR. Our estimated SAR model forcing is thus revised upwards by an amount
177 that increases linearly from zero in 1940 to 1.15 W/m² in 2040 and held constant afterwards (orange shading in right
178 panels of figure 1 and Extended Data Figure 6). The SAR runs we use are more useful than the CMIP1/2 simulations
179 for comparing to observations because the projected forcings over the 1990-2018 nowcast period are more similar to
180 our best guess of realized forcings over that period (see Historical Forcings section), due to the inclusion of both the
181 effect of increasing GHG concentrations and the direct effect of anthropogenic sulfate aerosol emissions (Figure 1,
182 right) [13].

183

184 We calculate democratic multi-model means by assigning an equal weight to each model version so as not to weight
185 models with several submitted runs (initial condition perturbation ensembles) more than other models. Weights are
186 also applied to all calculations of inter-model standard deviations ζ . Although we assign equal weights to each unique
187 model, these models should not be considered fully independent samples as many share similar codes, parameteriza-
188 tions, and tuning data sets [28]. The interdependence of models is evident in the grouping of global-mean surface air
189 temperature projections into two distinct branches corresponding to (upper) the North American models and (lower)
190 all other models (Extended Data Figure 6).

191 **IPCC Fifth Assessment Report (AR5) Models**

192 We compare GCMs from the SAR to a subset of models from the most recent generation of CMIP models (CMIP5)
193 from the IPCC's Fifth Assessment Report (AR5) run under the RCP 4.5 emissions scenario [53]. The AR5 model en-
194 semble includes: Five CanESM2 ensemble members from the Canadian Centre for Climate Modelling and Analysis;
195 Six CCSM4 ensemble members from the National Center for Atmospheric Research; Ten CSIRO-Mk3.6.0 ensemble
196 members from the Commonwealth Scientific and Industrial Research Organization in collaboration with Queensland
197 Climate Change Centre of Excellence; Five GISS-E2-H and six GISS-E2-R ensemble members from the NASA God-
198 dard Institute for Space Studies; One ensemble member each from ACCESS1.0 and ACCESS1.3 from the Common-
199 wealth Scientific and Industrial Research Organization and Bureau of Meteorology, Australia; One ensemble mem-
200 ber from BCC-CSM1.1 from the Beijing Climate Center, China Meteorological Administration; Four EC-EARTH
201 ensemble members from the EC-EARTH consortium; Two FIO-ESM ensemble members from the First Institute of
202 Oceanography, SOA, China; One ensemble member each from GFDL-CM3, GFDL-ESM2G and GFDL-ESM2M from
203 NOAA's Geophysical Fluid Dynamics Laboratory; One ensemble member each from HadGEM2-AO and HadGEM2-
204 CC from the Met Office Hadley Centre; Three MIROC5 ensemble members and one ensemble member each from
205 MIROC-ESM-CHEM and MIROC-ESM from the Atmosphere and Ocean Research Institute, National Institute for
206 Environmental Studies, and Japan Agency for Marine-Earth Science and Technology; One ensemble member from
207 MPI-ESM-LR from the Max-Planck-Institute for Meteorology; and one ensemble member each from NorESM1-M
208 and NorESM1-ME from the Norwegian Climate Centre. All models are linearly interpolated to a 3° latitude by 3°
209 longitude grid. The democratic multi-model mean is calculated by assigning an equal weight to each model version,
210 as described for SAR models above.

211 The AR5 multi-model mean (MMM) timeseries of global-mean temperature is shown in Extended Data Figure 6
212 (left) and the forcing timeseries associated with the RCP 4.5 scenario is shown in Extended Data Figure 6 (right). We
213 linearly interpolate the forcing between decadal averages to get an annually-resolved timeseries. Extended Data Figure
214 7 puts the SAR temperature trend forecast in the context of the more modern AR5 model forecast. Because the model
215 ensembles are forced differently over the forecast period (Extended Data Figure 6, right) and thus exhibit different
216 magnitudes of warming (assuming similar climate sensitivities), we normalize each model's spatially-resolved linear
217 temperature trends by its global-mean trend (Extended Data Figure 6, left). Extended Data Figure 7 C shows the
218 normalized spatial patterns of the AR5 MMM temperature trend and Extended Data Figure 7 D shows the ensemble
219 standard deviation ζ . The spatial patterns of MMM warming in the SAR and AR5 are similar, exhibiting comparable
220 degrees of Arctic amplification and enhanced warming over land relative to over ocean (Extended Data Figure 7 A and
221 C for SAR and AR5 MMMs, respectively; Extended Data Figure 3 for individual SAR models). A notable difference
222 is the lack of warming in the North Atlantic in AR5 (possibly related to differences in the slowdown of the AMOC
223 [16]). Inter-model variance in the spatial patterns of warming is smaller in AR5 than SAR over much of the globe
224 (Extended Data Figure 7 B, D).

225 **Observational Products**

226 We use the Berkeley Earth global product of surface air temperatures as observational ‘truth’ when assessing climate
227 models [5], because it is most independent of data products that may have been used for tuning the SAR models. To
228 quantify the uncertainty in the error metrics due to uncertainty in the observed temperatures, we also show the error
229 between the Berkeley Earth observations and the GISTEMP observations [54, 55] relative to the SAR median model
230 error (Figure 3).

231 Both the Berkeley Earth and GISTEMP observational products use sea surface temperatures as a proxy for surface
232 air temperature (SAT) over the ocean, where direct SAT measurements are sparse. This causes both observational
233 products to underestimate global-mean SAT trends by about 10% relative to estimates derived solely from SAT, such
234 as those presented here for SAR and AR5 models [56]. We mask trends in grid cells missing more than 50% of
235 monthly temperature values over the time period considered (e.g. over Antarctica in Extended Data Figure 2 B).

236 **Historical Forcings**

237 We estimate historical forcings and their uncertainties from a 200-member ensemble of adjusted forcings [57] di-
238 agnosed from historical CMIP5 simulations [53], updated for 2017 and linearly extrapolated out to 2018 (Figure 1,
239 right). These adjusted forcings represent our best guess of the radiative forcings over the 1920-1990 historical pe-
240 riod for which we have nearly global coverage of direct temperature observations. The adjusted forcings include the
241 combined effects of greenhouse gases, tropospheric aerosols, stratospheric aerosols (anthropogenic and volcanic), and
242 variations in solar forcing. Uncertainty in historical forcings is estimated by the inter-model standard deviation ζ (grey
243 shading in Figure 1, right).

244 **Spatially-resolved skill metrics**

245 Following [22], we measure a model m ’s skill based on the globally-averaged root mean square (RMS) error (E_m)
246 between a simulated field (F_m) and the observed field (R) from Berkeley Earth. We calculate three separate RMS
247 errors in order to distinguish between model skill at simulating: linear trends, annual-mean anomalies of the detrended
248 signal, and a climatology of seasonal cycles relative to their respective annual means. Relative errors (I_m) for a model
249 are calculated as

$$I_m = \frac{E_m - \bar{E}}{\bar{E}}, \quad (1)$$

250 where \bar{E} is the SAR multi-model median error. A model field is identical to the Berkeley Earth observations if $I_m = -1$,
251 agrees with Berkeley Earth better than the median SAR model if $-1 < I_m < 0$, and agrees with Berkeley Earth worse
252 than the median SAR model if $I_m > 0$. All relative errors I_m are shown in Extended Data Figure 4, with a subset shown
253 in Figure 3.

254 **Trend RMS error**

255 R_{ij} and F_{mij} are the linear trends in surface air temperatures (SATs) for latitude j , longitude i , and model m , calculated
 256 by linear regression of temperature against time over either the hindcast or nowcast period. We define

$$E_m^{(t)} = \sqrt{\frac{1}{W^{(t)}} \sum_i \sum_j w_{ij}^{(t)} \left(F_{mij}^{(t)} - R_{ij}^{(t)} \right)^2}, \quad (2)$$

257 where $w_{ij}^{(t)}$ are grid cell-area weights and $W^{(t)} = \sum_i \sum_j w_{ij}^{(t)}$ is the global surface area.

258 **Inter-annual RMS error**

259 R_{ijt} and F_{mijt} are the annual-mean SATs for year t , latitude j , longitude i , and model m , with the linear trend removed
 260 at each grid cell $[i, j]$ to isolate inter-annual variability from the linear trend. We define

$$E_m^{(a)} = \sqrt{\frac{1}{W^{(a)}} \sum_i \sum_j \sum_t w_{ijt}^{(a)} \left(F_{mijt}^{(a)} - R_{ijt}^{(a)} \right)^2}, \quad (3)$$

261 where $w_{ijt}^{(a)}$ are the grid cell-area weights and $W^{(a)} = \sum_i \sum_j \sum_t w_{ijt}^{(a)}$ is the global surface area times the number of years
 262 t .

263 **Seasonal Cycle RMS error**

264 R_{ijk} and F_{mijk} are the climatological SATs for month k , latitude j , longitude i , and model m . We remove the annual-
 265 mean temperature before computing the climatology in order to remove the combined effects of interannual variability
 266 and a linear trend. We define

$$E_m^{(s)} = \sqrt{\frac{1}{W^{(s)}} \sum_i \sum_j \sum_k w_{ijk}^{(s)} \left(F_{mijk}^{(s)} - R_{ijk}^{(s)} \right)^2}, \quad (4)$$

267 where $w_{ijk}^{(s)}$ is the product of the grid cell-area at grid cell $[i, j]$ and the length of the month k , and $W^{(s)} = \sum_i \sum_j \sum_k w_{ijk}^{(s)}$
 268 is the global surface area times the length of the year.

269 **Global-mean skill metric**

270 We define the global-mean trend metric (E_m) for a model m as the absolute difference between a simulated global-mean
 271 trend (F_m) and the observed global-mean trend (R) from Berkeley Earth,

$$E_m^{(g)} = |F_m - R|. \quad (5)$$

272 We define the relative global-mean trend error $I_m^{(g)}$ for a model m as

$$I_m^{(g)} = \frac{E_m^{(g)} - \overline{E^{(g)}}}{\overline{E^{(g)}}}, \quad (6)$$

273 where $\overline{E^{(g)}}$ is the SAR multi-model median error.

274 Data Availability

275 All data files for observational and model temperature fields and post-processing source code will be publicly available
276 at <https://github.com/hdrake/climate-model-performance> upon successful publication (or shared privately
277 beforehand upon request by reviewer).

278 References

- 279 [1] Stocker, T. *Climate change 2013: the physical science basis: Working Group I contribution to the Fifth assess-*
280 *ment report of the Intergovernmental Panel on Climate Change* (Cambridge University Press, 2014).
- 281 [2] Stouffer, R. J., Manabe, S. & Bryan, K. Interhemispheric asymmetry in climate response to a gradual increase
282 of atmospheric CO₂. *Nature* **342**, 660 (1989). URL <https://www.nature.com/articles/342660a0>.
- 283 [3] Reichler, T. & Kim, J. How Well Do Coupled Models Simulate Today's Climate? *Bulletin of the Amer-*
284 *ican Meteorological Society* **89**, 303–312 (2008). URL [https://journals.ametsoc.org/doi/10.1175/](https://journals.ametsoc.org/doi/10.1175/BAMS-89-3-303)
285 [BAMS-89-3-303](https://journals.ametsoc.org/doi/10.1175/BAMS-89-3-303).
- 286 [4] Houghton, J. T. *et al. Climate change 1995: The science of climate change: contribution of working group I to*
287 *the second assessment report of the Intergovernmental Panel on Climate Change*, vol. 2 (Cambridge University
288 Press, 1996).
- 289 [5] Rohde, R. *et al.* Berkeley Earth Temperature Averaging Process. *Geoinformat-*
290 *ics & Geostatistics: An Overview* **2013** (2016). URL [https://www.scitechnol.com/](https://www.scitechnol.com/berkeley-earth-temperature-averaging-process-IpUG.php?article_id=582)
291 [berkeley-earth-temperature-averaging-process-IpUG.php?article_id=582](https://www.scitechnol.com/berkeley-earth-temperature-averaging-process-IpUG.php?article_id=582).
- 292 [6] Medhaug, I., Stolpe, M. B., Fischer, E. M. & Knutti, R. Reconciling controversies about the ‘global warming
293 hiatus’. *Nature* **545** (2017).
- 294 [7] Eyring, V. *et al.* Taking climate model evaluation to the next level. *Nature Climate Change* **9**, 102 (2019). URL
295 <https://www.nature.com/articles/s41558-018-0355-y>.
- 296 [8] Summary for policymakers. In Masson-Delmotte, V. *et al.* (eds.) *Global Warming of 1.5C. An IPCC Special*
297 *Report on the impacts of global warming of 1.5C above pre-industrial levels and related global greenhouse gas*
298 *emission pathways, in the context of strengthening the global response to the threat of climate change, sustainable*
299 *development, and efforts to eradicate poverty* (World Meteorological Organization, Geneva, Switzerland, 2018).
- 300 [9] Hansen, J. *et al.* Global climate changes as forecast by Goddard Institute for Space Studies three-dimensional
301 model. *Journal of Geophysical Research: Atmospheres* **93**, 9341–9364 (1988). URL [https://agupubs.](https://agupubs.onlinelibrary.wiley.com/doi/abs/10.1029/JD093iD08p09341)
302 [onlinelibrary.wiley.com/doi/abs/10.1029/JD093iD08p09341](https://agupubs.onlinelibrary.wiley.com/doi/abs/10.1029/JD093iD08p09341).

- 303 [10] Hawkins, E. & Sutton, R. Time of emergence of climate signals. *Geophysical Research Letters* **39** (2012). URL
304 <https://agupubs.onlinelibrary.wiley.com/doi/abs/10.1029/2011GL050087>.
- 305 [11] Kiehl, J. T. & Shields, C. A. Climate simulation of the latest permian: Implications for mass extinction. *Geology*
306 **33**, 757–760 (2005).
- 307 [12] Allen, M. R., Stott, P. A., Mitchell, J. F. B., Schnur, R. & Delworth, T. L. Quantifying the uncertainty in fore-
308 casts of anthropogenic climate change. *Nature* **407**, 617 (2000). URL [https://www.nature.com/articles/](https://www.nature.com/articles/35036559)
309 [35036559](https://www.nature.com/articles/35036559).
- 310 [13] Mitchell, J. F. B., Johns, T. C., Gregory, J. M. & Tett, S. F. B. Climate response to increasing levels of greenhouse
311 gases and sulphate aerosols. *Nature* **376**, 501 (1995). URL <https://www.nature.com/articles/376501a0>.
- 312 [14] Boer, G. & Yu, B. Climate sensitivity and response. *Climate Dynamics* **20**, 415–429 (2003). URL <https://doi.org/10.1007/s00382-002-0283-3>.
313
- 314 [15] Smith, D. M. *et al.* Role of volcanic and anthropogenic aerosols in the recent global surface warming slowdown.
315 *Nature Climate Change* **6**, 936–940 (2016). URL <https://www.nature.com/articles/nclimate3058>.
- 316 [16] Caesar, L., Rahmstorf, S., Robinson, A., Feulner, G. & Saba, V. Observed fingerprint of a weakening At-
317 lantic Ocean overturning circulation. *Nature* **556**, 191 (2018). URL [https://www.nature.com/articles/](https://www.nature.com/articles/s41586-018-0006-5)
318 [s41586-018-0006-5](https://www.nature.com/articles/s41586-018-0006-5).
- 319 [17] Marshall, J. *et al.* The ocean’s role in the transient response of climate to abrupt greenhouse gas forcing. *Climate*
320 *Dynamics* **44**, 2287–2299 (2015).
- 321 [18] Jones, J. M. *et al.* Assessing recent trends in high-latitude Southern Hemisphere surface climate. *Nature Climate*
322 *Change* **6**, 917–926 (2016). URL <https://www.nature.com/articles/nclimate3103>.
- 323 [19] Collins, M. *et al.* Chapter 12 - Long-term climate change: Projections, commitments and irreversibility. In IPCC
324 (ed.) *Climate Change 2013: The Physical Science Basis. IPCC Working Group I Contribution to AR5* (Cam-
325 bridge University Press, Cambridge, 2013). URL [http://www.climatechange2013.org/images/report/](http://www.climatechange2013.org/images/report/WG1AR5_Chapter12_FINAL.pdf)
326 [WG1AR5_Chapter12_FINAL.pdf](http://www.climatechange2013.org/images/report/WG1AR5_Chapter12_FINAL.pdf).
- 327 [20] Pierce, D. W., Barnett, T. P., Santer, B. D. & Gleckler, P. J. Selecting global climate models for regional climate
328 change studies. *Proceedings of the National Academy of Sciences* **106**, 8441–8446 (2009). URL [https://www.](https://www.pnas.org/content/106/21/8441)
329 [pnas.org/content/106/21/8441](https://www.pnas.org/content/106/21/8441).
- 330 [21] Manabe, S., Stouffer, R. J., Spelman, M. J. & Bryan, K. Transient Responses of a Coupled Ocean–Atmosphere
331 Model to Gradual Changes of Atmospheric CO₂. Part I. Annual Mean Response. *Journal of Climate* **4**, 785–
332 818 (1991). URL [https://journals.ametsoc.org/doi/10.1175/1520-0442%281991%29004%3C0785%](https://journals.ametsoc.org/doi/10.1175/1520-0442%281991%29004%3C0785%3ATROACO%3E2.0.CO%3B2)
333 [3ATROACO%3E2.0.CO%3B2](https://journals.ametsoc.org/doi/10.1175/1520-0442%281991%29004%3C0785%3ATROACO%3E2.0.CO%3B2).

- 334 [22] Gleckler, P. J., Taylor, K. E. & Doutriaux, C. Performance metrics for climate models. *Journal of Geophysical*
335 *Research: Atmospheres* **113** (2008).
- 336 [23] Rauser, F., Gleckler, P. & Marotzke, J. Rethinking the Default Construction of Multimodel Climate Ensembles.
337 *Bulletin of the American Meteorological Society* **96**, 911–919 (2014). URL <https://journals.ametsoc.org/doi/10.1175/BAMS-D-13-00181.1>.
- 339 [24] Deser, C., Phillips, A. S., Alexander, M. A. & Smoliak, B. V. Projecting North American Climate over the Next
340 50 Years: Uncertainty due to Internal Variability. *Journal of Climate* **27**, 2271–2296 (2013). URL <https://journals.ametsoc.org/doi/full/10.1175/JCLI-D-13-00451.1>.
- 342 [25] Meehl, G. A. *et al.* Decadal Climate Prediction: An Update from the Trenches. *Bulletin of the American*
343 *Meteorological Society* **95**, 243–267 (2013). URL <https://journals.ametsoc.org/doi/full/10.1175/BAMS-D-12-00241.1>.
- 345 [26] Knutson, T. R., Delworth, T. L., Dixon, K. W. & Stouffer, R. J. Model assessment of regional surface temperature
346 trends (1949–1997). *Journal of Geophysical Research: Atmospheres* **104**, 30981–30996 (1999). URL <https://agupubs.onlinelibrary.wiley.com/doi/abs/10.1029/1999JD900965>.
- 348 [27] Knutson, T. R., Zeng, F. & Wittenberg, A. T. Multimodel Assessment of Regional Surface Temperature Trends:
349 CMIP3 and CMIP5 Twentieth-Century Simulations. *Journal of Climate* **26**, 8709–8743 (2013). URL <https://journals.ametsoc.org/doi/10.1175/JCLI-D-12-00567.1>.
- 351 [28] Knutti, R., Masson, D. & Gettelman, A. Climate model genealogy: Generation CMIP5 and how we got there.
352 *Geophysical Research Letters* **40**, 1194–1199 (2013). URL <https://agupubs.onlinelibrary.wiley.com/doi/abs/10.1002/grl.50256>.
- 354 [29] Schwartz, S. E., Charlson, R. J. & Rodhe, H. Quantifying climate change — too rosy a picture? *Nature Climate*
355 *Change* 23–24 (2007). URL <https://www.nature.com/articles/climate.2007.22>.
- 356 [30] Hourdin, F. *et al.* The Art and Science of Climate Model Tuning. *Bulletin of the American Meteorological Society*
357 **98**, 589–602 (2016). URL <https://journals.ametsoc.org/doi/full/10.1175/BAMS-D-15-00135.1>.
- 358 [31] Schmidt, G. A. *et al.* Practice and philosophy of climate model tuning across six US modeling centers. *Geosci-*
359 *entific Model Development* **10**, 3207–3223 (2017). URL <https://www.geosci-model-dev.net/10/3207/2017/gmd-10-3207-2017.html>.
- 361 [32] Braconnot, P. *et al.* Evaluation of climate models using palaeoclimatic data. *Nature Climate Change* **2**, 417–424
362 (2012). URL <https://www.nature.com/articles/nclimate1456>.
- 363 [33] Harrison, S. P. *et al.* Evaluation of cmip5 palaeo-simulations to improve climate projections. *Nature Climate*
364 *Change* **5**, 735 (2015).

- 365 [34] Burke, K. D. *et al.* Pliocene and Eocene provide best analogs for near-future climates. *Proceedings of the*
366 *National Academy of Sciences* **115**, 13288–13293 (2018). URL [https://www.pnas.org/content/115/52/](https://www.pnas.org/content/115/52/13288)
367 13288.
- 368 [35] Hansen, J., Lacic, A., Ruedy, R. & Sato, M. Potential climate impact of Mount Pinatubo eruption. *Geophysical*
369 *Research Letters* **19**, 215–218 (1992). URL [https://agupubs.onlinelibrary.wiley.com/doi/abs/10.](https://agupubs.onlinelibrary.wiley.com/doi/abs/10.1029/91GL02788)
370 1029/91GL02788.
- 371 [36] Parker, D. E., Wilson, H., Jones, P. D., Christy, J. R. & Folland, C. K. The Impact of
372 Mount Pinatubo on World-Wide Temperatures. *International Journal of Climatology* **16**, 487–497
373 (1996). URL [https://rmets.onlinelibrary.wiley.com/doi/abs/10.1002/%28SICI%291097-0088%](https://rmets.onlinelibrary.wiley.com/doi/abs/10.1002/%28SICI%291097-0088%28199605%2916%3A5%3C487%3A%3AAID-JOC39%3E3.0.CO%3B2-J)
374 28199605%2916%3A5%3C487%3A%3AAID-JOC39%3E3.0.CO%3B2-J.
- 375 [37] Stouffer, R. J. & Manabe, S. Assessing temperature pattern projections made in 1989. *Nature Climate Change*
376 **7**, 163–165 (2017). URL <https://www.nature.com/articles/nclimate3224>.
- 377 [38] Frame, D. J. & Stone, D. A. Assessment of the first consensus prediction on climate change. *Nature Climate*
378 *Change* **3**, 357–359 (2013). URL <https://www.nature.com/articles/nclimate1763>.
- 379 [39] Rahmstorf, S., Foster, G. & Cazenave, A. Comparing climate projections to observations up to 2011. *Envi-*
380 *ronmental Research Letters* **7**, 044035 (2012). URL [https://doi.org/10.1088%2F1748-9326%2F7%2F4%](https://doi.org/10.1088%2F1748-9326%2F7%2F4%2F044035)
381 2F044035.
- 382 [40] Cubasch, U. *et al.* Time-dependent greenhouse warming computations with a coupled ocean-atmosphere model.
383 *Climate Dynamics* **8**, 55–69 (1992). URL <https://doi.org/10.1007/BF00209163>.
- 384 [41] Hasselmann, K. F. *et al.* Detection of anthropogenic climate change using a fingerprint method (1995). URL
385 https://pure.mpg.de/pubman/faces/ViewItemOverviewPage.jsp?itemId=item_2534307.
- 386 [42] Roeckner, E. *et al.* The atmospheric general circulation model ECHAM4: Model description and simulation of
387 present-day climate. Report, Max-Planck-Institut für Meteorologie (1996). URL [http://centaur.reading.](http://centaur.reading.ac.uk/31813/)
388 [ac.uk/31813/](http://centaur.reading.ac.uk/31813/).
- 389 [43] Murphy, J. M. Transient Response of the Hadley Centre Coupled Ocean-Atmosphere Model to In-
390 creasing Carbon Dioxide. Part I: Control Climate and Flux Adjustment. *Journal of Climate* **8**, 36–56
391 (1995). URL [https://journals.ametsoc.org/doi/abs/10.1175/1520-0442%281995%29008%3C0036%](https://journals.ametsoc.org/doi/abs/10.1175/1520-0442%281995%29008%3C0036%3ATROTHC%3E2.0.CO%3B2)
392 3ATROTHC%3E2.0.CO%3B2.
- 393 [44] Murphy, J. M. & Mitchell, J. F. B. Transient Response of the Hadley Centre Coupled Ocean-Atmosphere Model
394 to Increasing Carbon Dioxide. Part II: Spatial and Temporal Structure of Response. *Journal of Climate* **8**, 57–
395 80 (1995). URL [https://journals.ametsoc.org/doi/10.1175/1520-0442%281995%29008%3C0057%](https://journals.ametsoc.org/doi/10.1175/1520-0442%281995%29008%3C0057%3ATROTHC%3E2.0.CO%3B2)
396 3ATROTHC%3E2.0.CO%3B2.

- 397 [45] Gordon, H. B. & O'Farrell, S. P. Transient Climate Change in the CSIRO Coupled Model with Dynamic Sea
398 Ice. *Monthly Weather Review* **125**, 875–908 (1997). URL [https://journals.ametsoc.org/doi/10.1175/
399 1520-0493\(1997\)125%3C0875%3ATCCITC%3E2.O.CO%3B2](https://journals.ametsoc.org/doi/10.1175/1520-0493(1997)125%3C0875%3ATCCITC%3E2.O.CO%3B2).
- 400 [46] Washington, W. M. & Meehl, G. A. High-latitude climate change in a global coupled ocean-atmosphere-sea
401 ice model with increased atmospheric CO₂. *Journal of Geophysical Research: Atmospheres* **101**, 12795–12801
402 (1996). URL <https://agupubs.onlinelibrary.wiley.com/doi/abs/10.1029/96JD00505>.
- 403 [47] Manabe, S. & Stouffer, R. J. Multiple-Century Response of a Coupled Ocean-Atmosphere Model to an Increase
404 of Atmospheric Carbon Dioxide. *Journal of Climate* **7**, 5–23 (1994). URL [https://journals.ametsoc.org/
405 doi/10.1175/1520-0442%281994%29007%3C0005%3AMCROAC%3E2.O.CO%3B2](https://journals.ametsoc.org/doi/10.1175/1520-0442%281994%29007%3C0005%3AMCROAC%3E2.O.CO%3B2).
- 406 [48] Boer, G. J. *et al.* Some results from an intercomparison of the climates simulated by 14 atmospheric general
407 circulation models. *Journal of Geophysical Research: Atmospheres* **97**, 12771–12786 (1992). URL [https://
408 //agupubs.onlinelibrary.wiley.com/doi/abs/10.1029/92JD00722](https://agupubs.onlinelibrary.wiley.com/doi/abs/10.1029/92JD00722).
- 409 [49] Flato, G. M. *et al.* The Canadian Centre for Climate Modelling and Analysis global coupled model and its
410 climate. *Climate Dynamics* **16**, 451–467 (2000). URL <https://doi.org/10.1007/s003820050339>.
- 411 [50] Tokioka, T. *et al.* A transient CO₂ experiment with the MRI CGCM - Annual mean response. Tech. Rep.
412 CGER–1022-96, National Institute for Environmental Studies (1996). URL [http://inis.iaea.org/Search/
413 search.aspx?orig_q=RN:39063264](http://inis.iaea.org/Search/search.aspx?orig_q=RN:39063264).
- 414 [51] Emori, S. *et al.* Coupled Ocean-Atmosphere Model Experiments of Future Climate Change with an Explicit
415 Representation of Sulfate Aerosol Scattering. *Journal of the Meteorological Society of Japan. Ser. II* **77**, 1299–
416 1307 (1999). URL [https://www.jstage.jst.go.jp/article/jmsj1965/77/6/77_6_1299/
_article](https://www.jstage.jst.go.jp/article/jmsj1965/77/6/77_6_1299/_article).
- 417 [52] Leggett, J. A., Pepper, W. J. & Swart, R. J. *Climate Change 1992. The Supplementary Report to the IPCC
418 Scientific Assessment.* (Cambridge University Press, 1992).
- 419 [53] Taylor, K. E., Stouffer, R. J. & Meehl, G. A. An Overview of CMIP5 and the Experiment Design. *Bulletin
420 of the American Meteorological Society* **93**, 485–498 (2011). URL [https://journals.ametsoc.org/doi/
421 abs/10.1175/BAMS-D-11-00094.1](https://journals.ametsoc.org/doi/abs/10.1175/BAMS-D-11-00094.1).
- 422 [54] Hansen, J., Ruedy, R., Sato, M. & Lo, K. Global surface temperature change. *Reviews of Geophysics* **48** (2010).
423 URL <https://agupubs.onlinelibrary.wiley.com/doi/full/10.1029/2010RG000345>.
- 424 [55] Team, G. Giss surface temperature analysis (gistemp). <https://data.giss.nasa.gov/gistemp/>. Accessed:
425 2019-03-15.
- 426 [56] Cowtan, K. *et al.* Robust comparison of climate models with observations using blended land air and ocean
427 sea surface temperatures. *Geophysical Research Letters* **42**, 6526–6534 (2015). URL [https://agupubs.
428 onlinelibrary.wiley.com/doi/10.1002/2015GL064888](https://agupubs.onlinelibrary.wiley.com/doi/10.1002/2015GL064888).

429 [57] Forster, P. M. *et al.* Evaluating adjusted forcing and model spread for historical and future scenarios in the CMIP5
430 generation of climate models. *Journal of Geophysical Research: Atmospheres* **118**, 1139–1150 (2013). URL
431 <https://agupubs.onlinelibrary.wiley.com/doi/10.1002/jgrd.50174>.

432 **Acknowledgements**

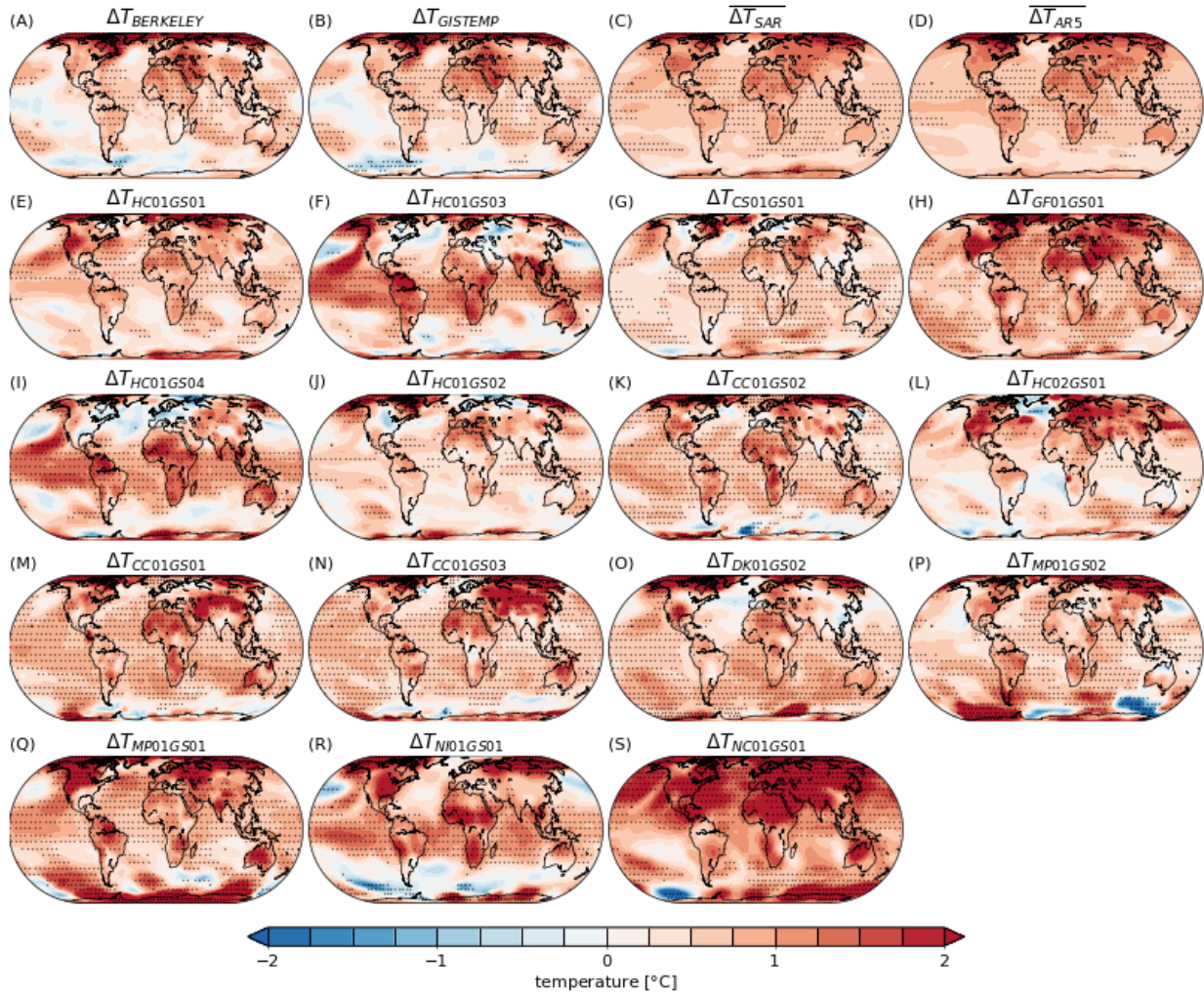
433 We acknowledge the World Climate Research Programme’s Working Group on Coupled Modelling, which is respon-
434 sible for CMIP, and we thank the climate modeling groups for producing and making available their model output. For
435 CMIP the U.S. Department of Energy’s Program for Climate Model Diagnosis and Intercomparison provides coordi-
436 nating support and led development of software infrastructure in partnership with the Global Organization for Earth
437 System Science Portals. We thank Susan Solomon and Nick Lutsko for feedback on an earlier draft of the manuscript.

438 **Author Contributions**

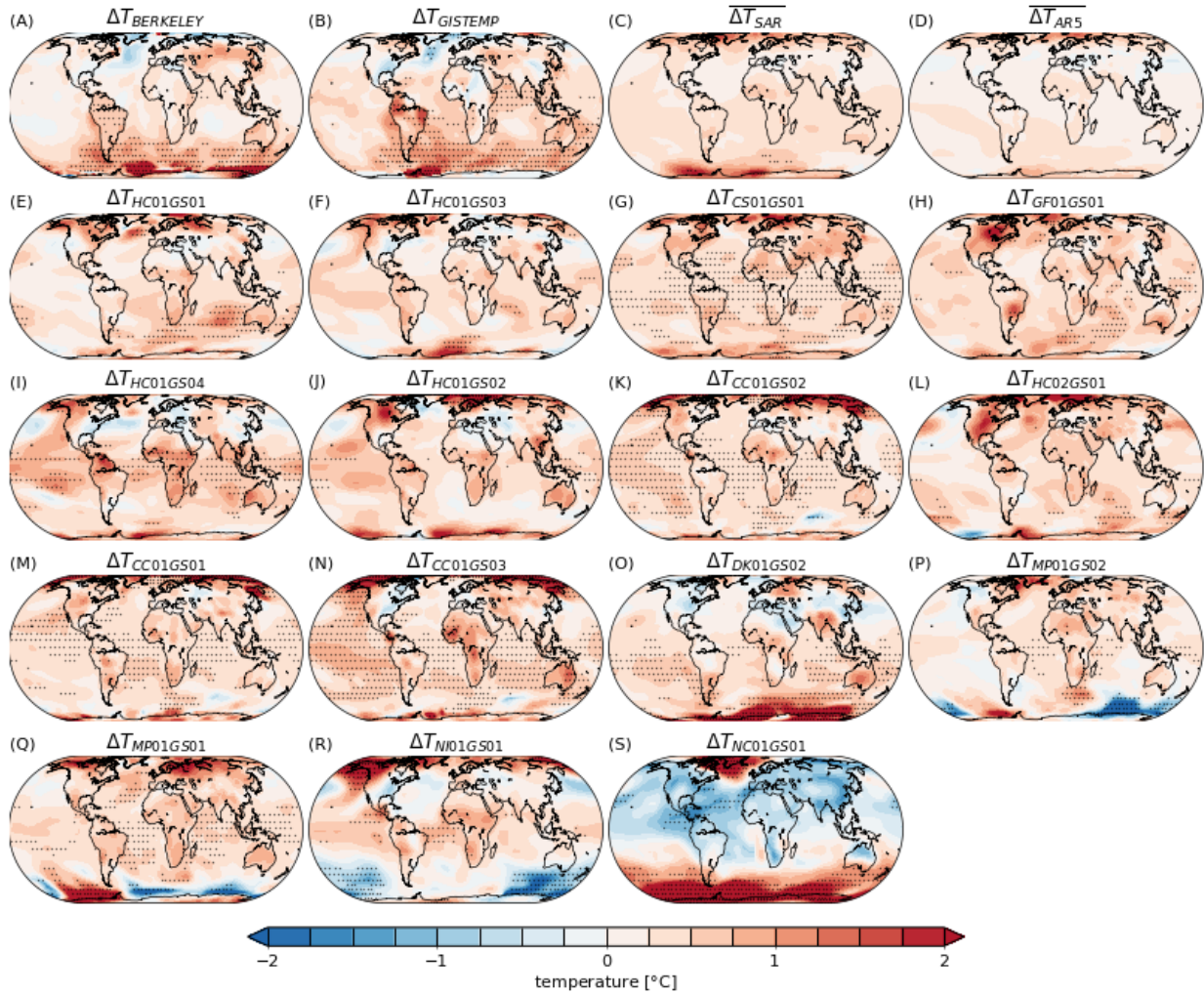
439 All authors interpreted the data and wrote the paper. H.F.D. and T.A. conceived of the work; H.F.D. performed the
440 data analysis.

441 **Author Information**

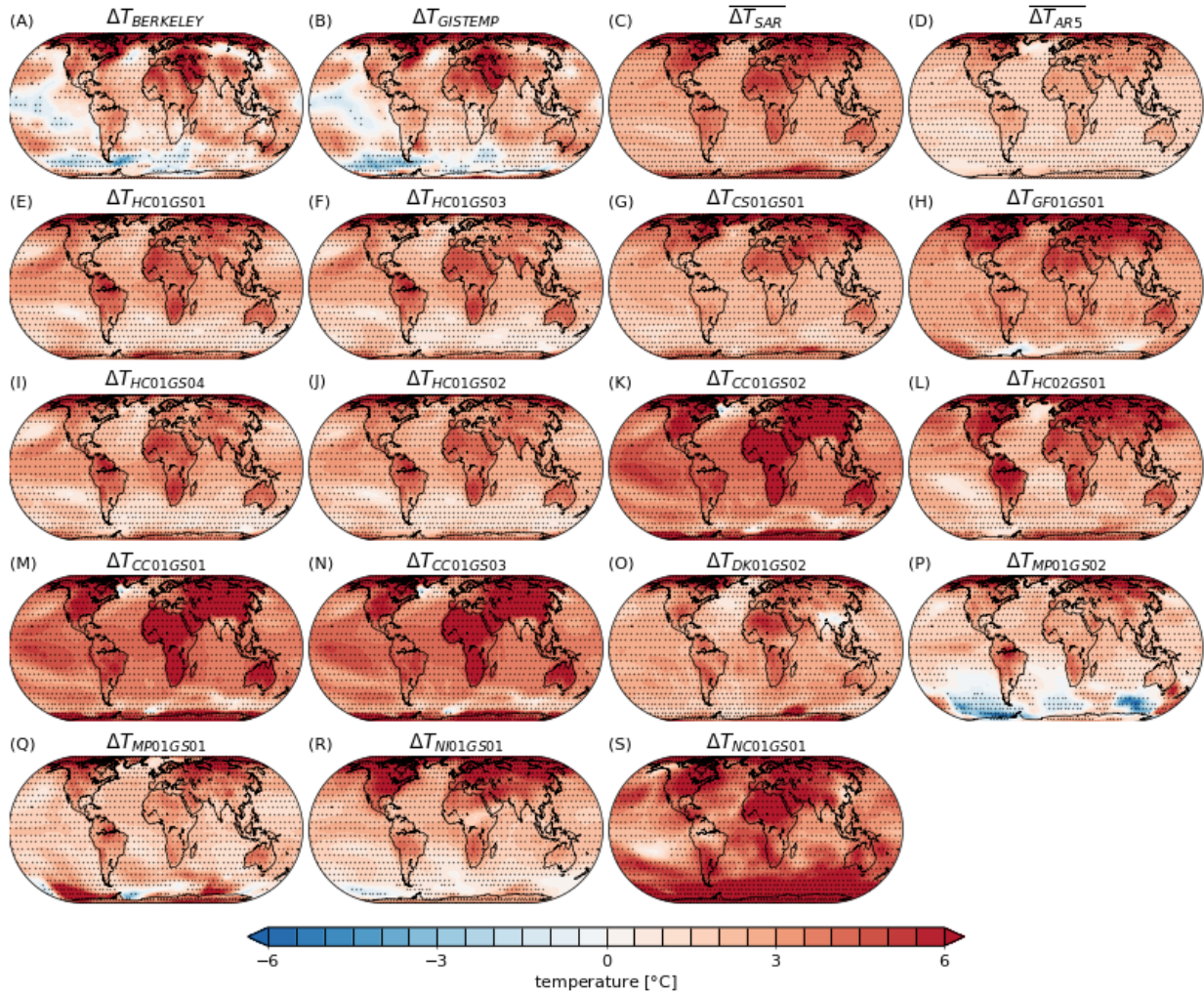
442 Reprints and permissions information is available at www.nature.com/reprints. The authors declare no competing
443 interests. Correspondence and requests for materials should be addressed to henrifdrake@gmail.com.



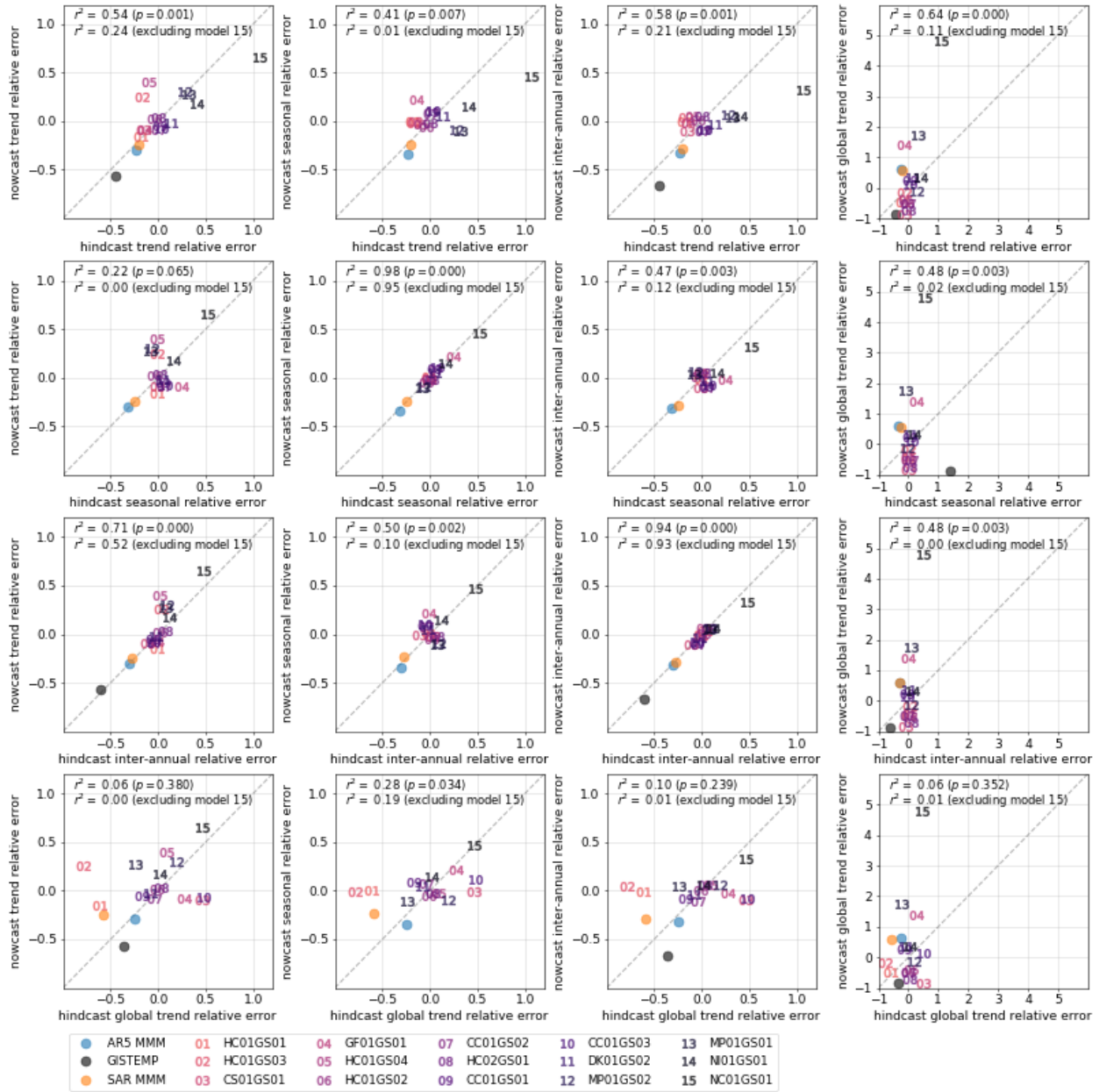
Extended Data Figure 1: Projected and observed spatial patterns of warming trends over the 1990-2018 nowcast period for (A) the Berkeley Earth observations, (B) the GISTEMP observations, (C) the SAR multi-model mean, (D), the AR5 multi-model mean, and (E-S) each individual SAR model. Stippling shows where the absolute temperature trend signal has emerged above the noise of inter-annual variability, $|\Delta T| > 2\sigma$, where σ is defined as the standard deviation of the annual-mean temperature timeseries with the nowcast linear trend removed, for each product. See Figure 2 for trends over the 1920-1990 hindcast period and Figure 3 for trends over the 1990-2100 forecast period.



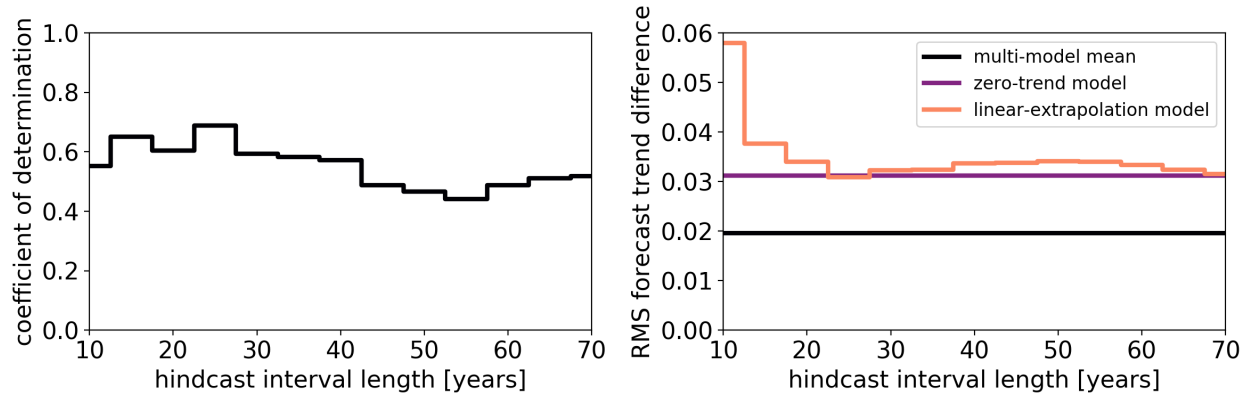
Extended Data Figure 2: Projected and observed spatial patterns of warming trends over the 1920-1990 hindcast period for (A) the Berkeley Earth observations, (B) the GISTEMP observations, (C) the SAR multi-model mean, (D), the AR5 multi-model mean, and (E-S) each individual SAR model. Stippling shows where the absolute temperature trend signal has emerged above the noise of inter-annual variability, $|\Delta T| > 2\sigma$, where σ is defined as the standard deviation of the annual-mean temperature timeseries with the hindcast linear trend removed, for each product.



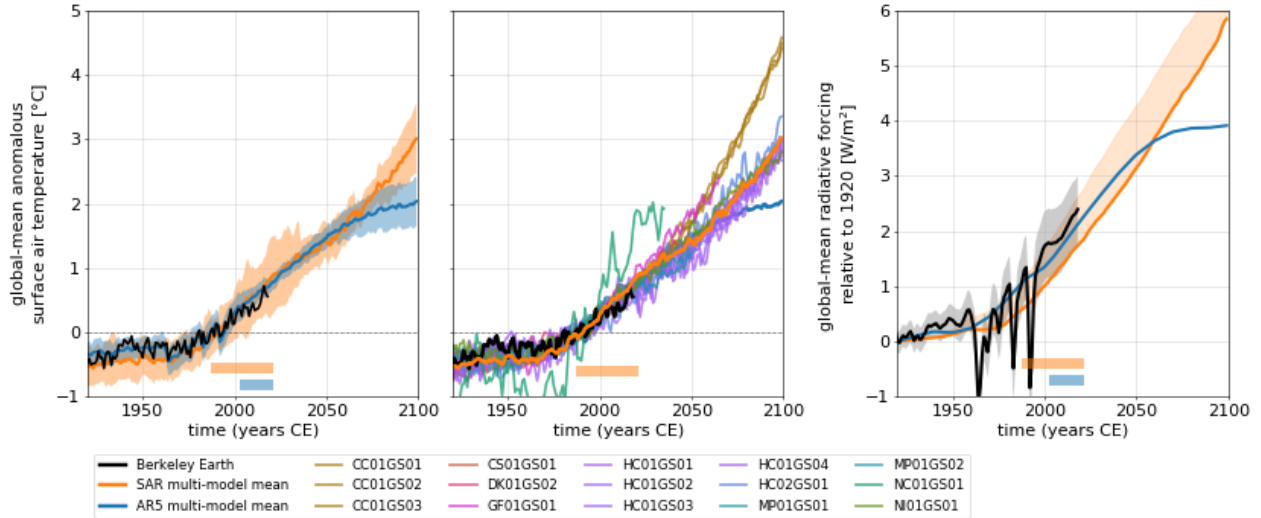
Extended Data Figure 3: Projected and observed spatial patterns of warming trends over the 1990-2100 forecast period for (A) the Berkeley Earth observations, (B) the GISTEMP observations, (C) the SAR multi-model mean, (D), the AR5 multi-model mean, and (E-S) each individual SAR model. For the observations (A) and (B), we linearly extrapolate the 1990-2018 nowcast trend for heuristic comparison with models. Stippling shows where the absolute temperature trend signal has emerged above the noise of inter-annual variability, $|\Delta T| > 2\sigma$, where σ is defined as the standard deviation of the annual-mean temperature timeseries with the forecast linear trend removed, for each product.



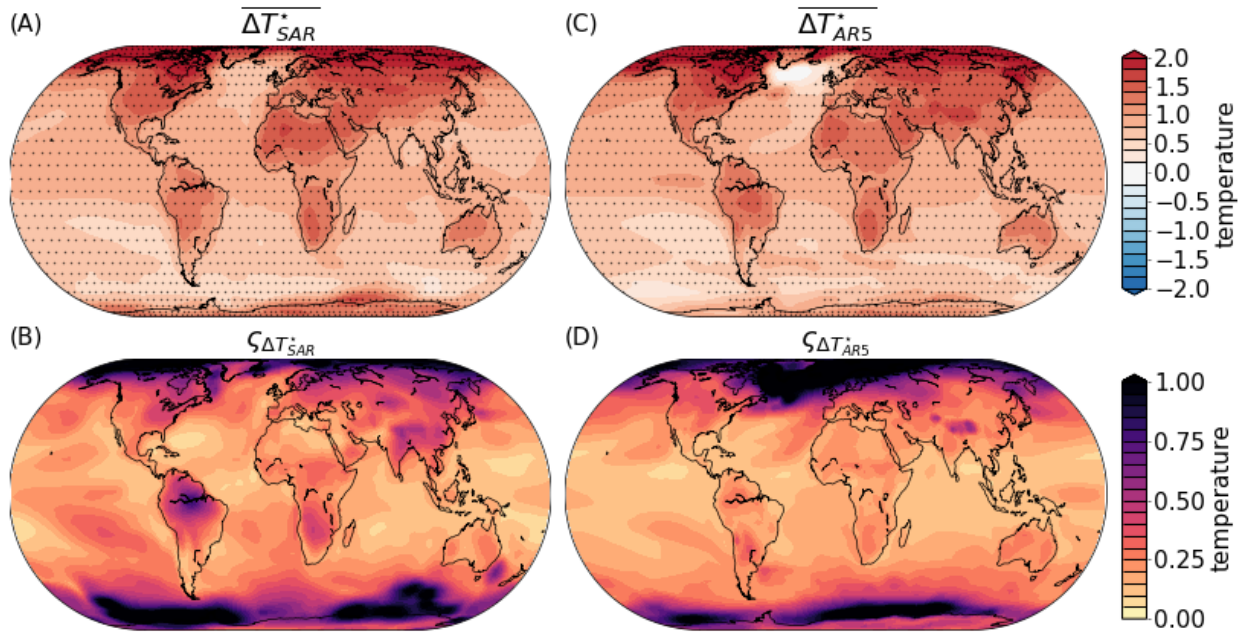
Extended Data Figure 4: Correlations between skill metrics for 1920-1990 hindcast and 1990-2018 nowcast. Y-axes show the skill metrics for the nowcast and x-axes show skill metrics for the hindcast. The four skill metrics shown are: (A) a spatially-resolved temperature trend metric, (B) a temperature seasonality metric, (C) an inter-annual temperature variability metric, and (D) a global-mean temperature trend metric. Large negative values indicate high model skill (see Methods for details). We show (blue) the AR5 multi-model mean, (black) the GISTEMP observations, (orange) the SAR multi-model mean, and (1-15) each individual model. Coefficients of determination r^2 are calculated (upper) by excluding GISTEMP and AR5 MMM and (lower) additionally excluding the outlier model NC01GS01. Note the change in axis scales for the right-most column.



Extended Data Figure 5: (Left) Coefficients of determination for nowcast trend relative error against hindcast trend relative error (e.g. Figure 3A, upper) as a function of hindcast interval length (all ending in 1990). (Right) Root-mean square difference between model trend forecast and Berkeley Earth trend forecast for the multi-model mean and two heuristic reference cases: a uniformly-zero trend case and a linear extrapolation case. The hindcast interval length (always ending at 1990) is varied from 10 years to 70 years to show that the relative skill of the multi-model mean to the extrapolation case is independent of the period over which the hindcast trend is calculated.



Extended Data Figure 6: Projected and observed global annual mean surface air temperature anomalies and radiative forcing. (Left) Global annual mean surface air temperature anomalies relative to the 1985-1995 mean. Solid lines show the (black) Berkeley Earth observations, (orange) SAR multi-model mean, (blue) AR5 multi-model mean. Orange and blue shading show the SAR and AR5 multi-model means $\pm\zeta$, respectively, where ζ is the inter-model standard deviation. (Middle) Global annual mean surface air temperature anomalies relative to the 1985-1995 mean for each individual SAR model where colors indicate different models. (Right) Global mean radiative forcing relative to 1920. Solid lines show our estimates of historical, SAR model, and AR5 (following the RCP4.5 scenario) forcing and the shading shows uncertainty estimates (see Methods for details). The orange bars delineate the 1990-2018 SAR nowcast period and the blue bars delineate the 2005-2018 AR5 nowcast period. Note that the abrupt decrease in SAR model spread around 2033 in the left panel is due to the end of the outlier projection from the NC01GS01 model.



Extended Data Figure 7: (Left) Multi-model mean spatial patterns of normalized temperature trends over the 1990-2100 forecast period for the (A) SAR and the (C) AR5. Stippling shows where the multi-model mean absolute temperature change $|\Delta T|$ is more than twice the multi-model mean inter-annual variability σ (as in Figure 2). (Right) Inter-model standard deviation ζ of the normalized temperature trends for the (B) SAR and the (D) AR5. Each individual model's temperature trends are normalized by its global mean temperature trend.